Motor neuron disease, TDP-43 pathology, and memory deficits in mice expressing ALS–FTD-linked *UBQLN2* mutations

Nhat T. T. Le[a,b,1], Lydia Chang[a,b,1], Irina Kovlyagina[a,b,1], Polymnia Georgiou[c], Nathaniel Safren[a,b], Kerstin E. Braunstein[d], Mark D. Kvarta[e], Adam M. Van Dyke[e], Tara A. LeGates[e], Thomas Philips[f,g], Brett M. Morrison[f,g], Scott M. Thompson[e], Adam C. Puche[b], Todd D. Gould[b,c], Jeffrey D. Rothstein[f,g], Philip C. Wong[d], and Mervyn J. Monteiro[a,b,2]

[a]Center for Biomedical Engineering and Technology, University of Maryland School of Medicine, Baltimore, MD 21201; [b]Department of Anatomy and Neurobiology, University of Maryland School of Medicine, Baltimore, MD 21201; [c]Department of Psychiatry, University of Maryland School of Medicine, Baltimore, MD 21201; [d]Department of Pathology and Neuroscience, The Johns Hopkins University School of Medicine, Baltimore, MD 21287; [e]Department of Physiology, University of Maryland School of Medicine, Baltimore, MD 21201; [f]Brain Science Institute, The Johns Hopkins University School of Medicine, Baltimore, MD 21287; and [g]Department of Neurology, The Johns Hopkins University School of Medicine, Baltimore, MD 21287

Edited by Don W. Cleveland, University of California at San Diego, La Jolla, CA, and approved October 13, 2016 (received for review May 25, 2016)

Missense mutations in *ubiquilin 2* (*UBQLN2*) cause ALS with frontotemporal dementia (ALS–FTD). Animal models of ALS are useful for understanding the mechanisms of pathogenesis and for preclinical investigations. However, previous rodent models carrying *UBQLN2* mutations failed to manifest any sign of motor neuron disease. Here, we show that lines of mice expressing either the ALS–FTD-linked P497S or P506T *UBQLN2* mutations have cognitive deficits, shortened lifespans, and develop motor neuron disease, mimicking the human disease. Neuropathologic analysis of the mice with end-stage disease revealed the accumulation of ubiquitinated inclusions in the brain and spinal cord, astrocytosis, a reduction in the number of hippocampal neurons, and reduced staining of TAR-DNA binding protein 43 in the nucleus, with concomitant formation of ubiquitin$^+$ inclusions in the cytoplasm of spinal motor neurons. Moreover, both lines displayed denervation muscle atrophy and age-dependent loss of motor neurons that correlated with a reduction in the number of large-caliber axons. By contrast, two mouse lines expressing WT *UBQLN2* were mostly devoid of clinical and pathological signs of disease. These *UBQLN2* mouse models provide valuable tools for identifying the mechanisms underlying ALS–FTD pathogenesis and for investigating therapeutic strategies to halt disease.

ALS | motor neuron disease | UBQLN2 | TDP-43 pathology

ALS is a progressive neurodegenerative disorder associated with loss of upper and lower motor neurons (1, 2). The disease usually manifests in the fifth decade of life, but can occur as early as the late teens. Its hallmark symptoms are progressive muscle weakness, which usually leads to death between 3 and 5 y after first diagnosis. Some patients with ALS also develop frontotemporal dementia (FTD). Genetic findings have linked mutations in different genes to the range of symptoms seen in ALS (3, 4).

A common pathologic feature in nearly all ALS cases (~97%), including all sporadic and most familial cases, is a reduction in TAR-DNA binding protein 43 (TDP-43) in the nucleus and its accumulation in ubiquitin$^+$ inclusions in the cytoplasm of spinal motor neurons (5–8). The few exceptions where this pathology is not seen are in ALS cases linked to mutations in the *SOD1* and *FUS* genes (7–10). This has led to speculation that pathogenesis in the vast majority of ALS cases may be mechanistically linked directly or indirectly to TDP-43 pathology (7, 11). Intriguingly, TDP-43 pathology is also a common hallmark of certain forms of FTD where the pathology is found in the brain (5, 7, 12).

Missense mutations (P497H, P497S, P506T, P509S, or P525S) in *ubiquilin 2* (*UBQLN2*) were identified as the cause of X-linked dominant ALS–FTD (13). The afflicted individuals had abnormal inclusions in neurons of the hippocampus and TDP-43 pathology in spinal motor neurons. Additional *UBQLN2* mutations have now been identified, and interestingly, like the original mutations, encode missense mutations in the central domain of UBQLN2 protein (14–16). The function of the central domain of UBQLN2 is beginning to emerge with studies showing it assists in chaperone function (17–19) and in docking the protein with different adaptors of its function (20–22). The function of the two end domains that border the central domain is better understood. At the N terminus is a UBL domain that binds the proteasome and at the C terminus a UBA domain that binds ubiquitin moieties typically tagged onto proteins targeted for degradation. Their properties fit with the function of UBQLN proteins as shuttle factors that bind and deliver misfolded proteins to the proteasome for degradation (23, 24). In addition to proteasomal degradation, UBQLN proteins also play a role by facilitating autophagy (25, 26).

The mechanisms by which *UBQLN2* mutations cause ALS are not completely understood. Knockout of the *UBQLN2* gene in rat produced no overt phenotype, ruling out simple loss of function (27). Therefore, it can be postulated that *UBQLN2* mutations result in ALS endophenotypes through a gain-of-function

Significance

Animal models of human diseases provide important tools for mechanistic and preclinical investigations. Mutations in several genes cause ALS. One such gene is *ubiquilin 2* (*UBQLN2*), mutations in which cause dominant inheritance of ALS with frontotemporal dementia (ALS–FTD). Several rodent models carrying *UBQLN2* mutations have been described, but none develop motor neuron disease. We describe two transgenic (Tg) mouse models of ALS–FTD carrying different *UBQLN2* mutations. Both models develop cognitive deficits, classic TAR-DNA binding protein 43 (TDP-43) pathology seen in ALS, and motor neuron disease. By contrast, Tg mouse lines expressing WT UBQLN2 had normal lifespans, no evidence of TDP-43 pathology, and mild signs of disease. These mouse lines provide valuable investigative tools for ALS–FTD research.

Author contributions: N.T.T.L. and M.J.M. designed research; N.T.T.L., L.C., I.K., P.G., N.S., K.E.B., M.D.K., A.M.V.D., T.A.L., T.P., B.M.M., S.M.T., A.C.P., and M.J.M. performed research; N.T.T.L., P.G., N.S., K.E.B., M.D.K., A.M.V.D., T.A.L., T.D.G., J.D.R., P.C.W., and M.J.M. analyzed data; and N.T.T.L. and M.J.M. wrote the paper.

The authors declare no conflict of interest.

This article is a PNAS Direct Submission.

[1]N.T.T.L., L.C., and I.K. contributed equally to this work.

[2]To whom correspondence should be addressed. Email: monteiro@umaryland.edu.

This article contains supporting information online at www.pnas.org/lookup/suppl/doi:10.1073/pnas.1608432113/-/DCSupplemental.

and/or through a dominant-negative mechanism. Indeed, overexpression of the mutant UBQLN2 (mtUBQLN2) proteins in cells and animals support both possibilities. For example, overexpression of ALS mtUBQLN2 proteins caused interference in proteasomal degradation, including perturbation of endoplasmic reticulum-associated degradation (ERAD) (13, 28–31). The interference in degradation appears to stem from an inability of the mutants to deliver polyubiquitinated proteins to the proteasome for degradation (30, 32). The defective delivery could account for buildup of ubiquitin^{+} UBQLN2 inclusions seen in the disease. The accumulation of UBQLN2 inclusions could be interpreted as a gain of function. On the other hand, it could signify a loss of function, because UBQLN proteins function in autophagy, which typically involves clearance of large aggregates. Other studies have shown ALS–FTD *UBQLN2* mutations reduce binding of UBQLN2 with its normal partners, suggesting a possible loss of function (19, 22, 28). Evidently, understanding how *UBQLN2* mutations cause ALS–FTD is important for understanding the mechanisms underlying the disease and for developing novel pharmacotherapies to halt the disease. Models that faithfully recapitulate key aspects of the disease would be valuable tools toward these goals.

Several rodent models of UBQLN2 have been developed. A mouse or rat transgenic (Tg) model expressing the P497H *UBQLN2* mutation was found to possess memory deficits, but did not develop motor neuron disease (27, 29). In both lines UBQLN puncta were found in the hippocampus in a pattern similar to that seen in humans carrying *UBQLN2* mutations. A P520T knockin mouse model, carrying the equivalent P506T *UBQLN2* mutation in humans, developed cognitive deficits and UBQLN2 inclusions in the brain, but did not develop motor neuron disease (19). Other studies showed that mice injected with adeno-associated virus (AAV) expressing the P497S and P506T *UBQLN2* mutations perform worse on the rotarod than mice expressing WT UBQLN2 or the P497H mutation (31). However, the underlying reason for the variation in their motor performance was not described. Here we describe lines of mice that express either WT or ALS–FTD mutant P497S or P506T human UBQLN2 (hUBQLN2) proteins. We show the mice lines expressing the mutant hUBQLN2 proteins not only develop memory deficits and motor neuron disease, but also display the pathological hallmarks of the disease found in humans. The behavioral, biochemical, and pathological characterization of the lines are presented, showing they could be valuable models for ALS–FTD research.

Results

Generation of Lines of Mice Expressing WT and ALS–FTD mtUBQLN2 Proteins. cDNA encoding either full-length untagged WT human UBQLN2 or the ALS–FTD P497S or P506T missense mutants were cloned into the neuron-specific Thy1.2 expression cassette (33) and mouse lines carrying between one and five copies for each construct were established (Fig. 1*A* and *SI Appendix*, Fig. S1 *A* and *B*). The Tg hUBQLN2 protein expressed in the lines was distinguishable from the endogenous mouse UBQLN2 (mUBQLN2) protein by immunoblot analysis (Fig. 1*B*). Mouse lines WT-356, P497S_3, and P506T_6 (the latter two henceforth referred to simply as P497S and P506T) that by immunoblot analysis of spinal cord (SC) lysates of 1-mo-old animals expressed similar levels of the corresponding Tg hUBQLN2 proteins, were characterized clinically, behaviorally, and pathologically to see whether they developed any ALS–FTD syndromes. In these lines, hUBQLN2 protein was overexpressed to ∼70–80% the level of endogenous mUBQLN2 (Fig. 1*C*). An additional line, called WT-358, expressing WT hUBQLN2 to ∼20% the level of mUBQLN2, was also studied. Immunoblots of different brain regions revealed the transgenes in all four lines were expressed in the brainstem,

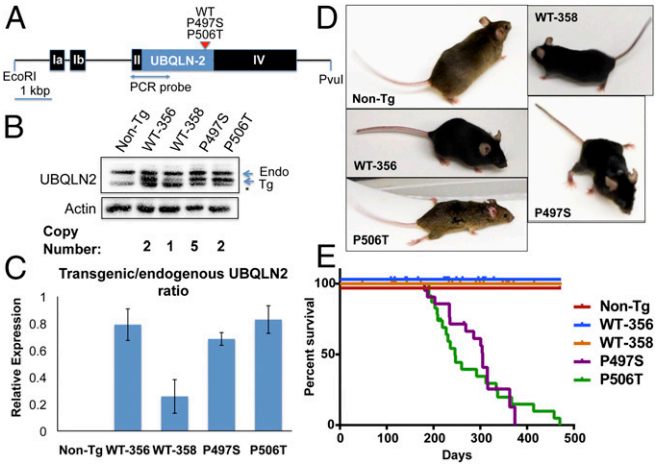

Fig. 1. Generation of UBQLN2 Tg mice. (*A*) Schematic of the Thy1.2 expression constructs in which untagged human UBQLN2 cDNA encoding either WT or the ALS–FTD P497S or P506T mutants were used to generate Tg mice. (*B*) SC lysates from 1-mo-old animals immunoblotted with a UBQLN2-specific antibody and actin for a loading control. The arrows indicate the position of the endogenous (Endo, *Upper*) and Tg human UBQLN2 protein (*Lower*) bands. The * corresponds to an unknown band. (*C*) Quantification of the ratio of human to mouse UBQLN2 bands found in SC lysates of 1-mo-old mice. (*D*) Still photos of live 1-y-old WT 356 and WT-358 animals, two 11-mo-old non-Tg and Tg P506T littermates, and a 7-mo-old Tg P497S animal. Note hindleg paralysis in the mutant Tg animals. (*E*) Survival curves for the WT, mutant, and non-Tg UBQLN2 mice based on the following number of animals: WT-356, 20; WT-358, 24; P497S, 21; P506T, 23; and non-Tg,19.

cortex, hippocampus, striatum, and cortex, with lower expression in the cerebellum (*SI Appendix*, Fig. S1*C*).

All of the mice belonging to the P497S and P506T lines developed progressive difficulty in movement (Movies S1–S6), an increase in forelimb and hindlimb clasping and several (∼40%) P506T animals and a few (∼10%) of the P497S animals developed hindleg paralysis (Fig. 1*D*). They all had to be killed at various ages as they reached end-point criteria. By contrast, neither the nontransgenic (non-Tg) littermates nor any of the lines expressing WT hUBQLN2 manifested similar phenotypes, with all them surviving the entire period of study. The survival curves for the different lines are shown in Fig. 1*E*. Median survival for the P506T and P497S lines was 246 and 305 d, respectively. Median survival for the two WT lines was undefined, but estimated to be similar to non-Tg animals.

Expression of Mutant, but Not WT UBQLN2 Proteins in Neuronal Tissues Leads to Age-Dependent Accumulation of UBQLN2 Inclusions in the Brain and SC. We used immunohistochemistry to examine UBQLN2 staining in the brain and SC of the Tg and non-Tg animals. The brain staining revealed the presence of numerous UBQLN2^{+} inclusions in both end-stage P497S and P506T lines (Fig. 2*A*). Such inclusions were rarely seen in the brains of equivalent age WT UBQLN2-expressing lines or in non-Tg animals, where instead UBQLN2 staining was more uniform (Fig. 2 *A*, *d–f*). The distribution pattern of the inclusions in P497S and P506T animals was remarkably similar. In both lines, inclusions were particularly prominent in layers V–VI of the cortex (positive for Ctip-2), in the inner and middle molecular layers of the dentate gyrus, the cornus ammonis 1 (CA1) region of the hippocampus, in the brainstem, and striatum (Fig. 2 *A* and *B*). The striking pattern of UBQLN2 inclusions in the dentate gyrus of the mutant mice was adjacent to the granular layer (Fig. 2 *B*, *b* and *c*). Its distribution is very similar to that found in human carriers of *UBQLN2* mutations and in the two P497H *UBQLN2* rodent models previously described (13, 27, 29). Double immunofluorescence microscopy indicated

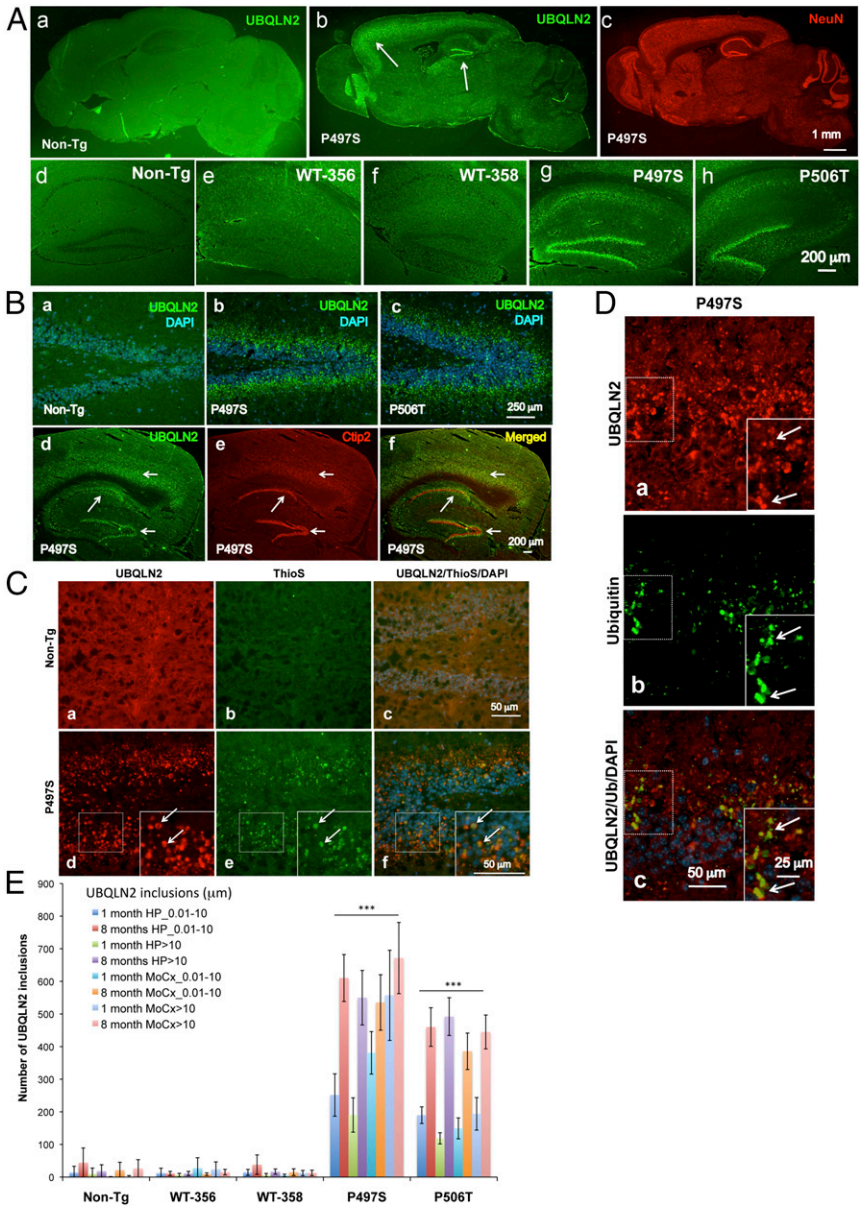

Fig. 2. Formation and properties of UBQLN inclusions in the brain of mtUBQLN2 mice. Phenotypic, behavioral, and survival properties of UBQLN2 mice. (*A*) Sagittal sections of whole mouse brain from end-stage (~12 mo) P497S and an age-matched non-Tg animal stained for UBQLN2 (*a* and *b*). The section in *b* was counterstained with NeuN (*c*). The arrows (in *b*) indicate prominent staining of puncta in the dentate gyrus and cortex. (*d–h*) Staining of UBQLN2 in the hippocampus of 8-mo-old animals for the genotypes shown. (*B*) Double staining of UBQLN2 and DAPI to show the disposition of UBQLN2 puncta in the dentate gyrus (*a–c*). Double staining of the hippocampal region for UBQLN2 and Ctip2 to show the overlap between the two signals (*d–f*). (*C*) Double staining of the dentate gyrus of an 8-mo-old non-Tg (*a–c*) and P497S Tg (*d–f*) for thioflavin S and UBQLN2. The area outlined with dashes is enlarged to easily see the colocalization (arrows). (*D*) Double immunofluorescence staining of UBQLN2 and ubiquitin demonstrating some of the UBQLN2 inclusions are strongly positive for ubiquitin. (*E*) Quantification of UBQLN2 inclusions (separated into two size classes) in the motor cortex and hippocampus in the different lines at 1 and 8 mo of age. Data shown is the mean ± SD.

many of the UBQLN2 inclusions costain with ubiquitin (Fig. 2*D*) and thioflavin S (Fig. 2*C*), suggesting they constitute ubiquitinated proteins with amyloid conformation.

Comparison of UBQLN2 staining in the hippocampus of 1-, 3-, and 8-mo-old animals revealed an age-dependent deposition of inclusions in the mutant animals (*SI Appendix*, Fig. S2). We quantified the number and size of UBQLN2 inclusions in the hippocampus and motor cortex regions of the brains of 1- and 8-mo-old Tg and non-Tg mice. The quantification revealed an age-dependent increase in the number of both small- and large-size UBQLN2 inclusions in both P497S and P506T mutant lines (Fig. 2*E*). Interestingly, P497S animals contained more inclusions than P506T animals at both ages analyzed. By contrast, the number of inclusions in the two WT UBQLN2 lines was considerably lower and similar in number to those found in non-Tg animals at the two ages examined.

Staining of SC sections revealed a similar age-dependent accumulation of UBQLN2 inclusions in both early (1 mo of age) and end-stage (~8 mo of age) P497S and P506T animals, and like the brain, few such inclusions were present in any of the age-matched WT UBQLN2 and non-Tg animals (Fig. 3 *A* and *B*). Some of the end-stage mtUBQLN2 mice contained very large irregular-shaped structures in the gray matter that stained strongly with the UBQLN2 antibody (Fig. 3*A* and *SI Appendix*, Fig. S3 *A* and *B*). These large UBQLN2^{+} structures were negative for glial fibrillary acidic protein (GFAP) (*SI Appendix*, Fig. S3*A*) and ionized calcium-binding adaptor molecule 1 (Iba1) (*SI Appendix*, Fig. S3*B*) staining, suggesting they are unlikely to be microglia or astrocytes.

Because previous studies suggested ALS–FTD P497S and P506T mutant UBQLN2 proteins have slower turnover than the WT protein (30), we examined SC lysates of the Tg mice to see whether accumulation of the Tg hUBQLN2 proteins is altered in older mice. As shown in Fig. 1*B*, at 1 mo of age there was little difference in the levels of the expressed mutant and WT UBQLN2 Tg proteins in P497S, P506T, and WT-356 lines. However, at 8 mo of age, we found the levels of the Tg mutant hUBQLN2 proteins in both P497S and P506T animals were increased compared with the level of WT hUBQLN2 protein in the WT-356 line (Fig. 3 *C* and *D* and *SI Appendix*, Fig. S3*C*). Moreover, the level of endogenous mUBQLN2 was elevated in both end-stage P497S and

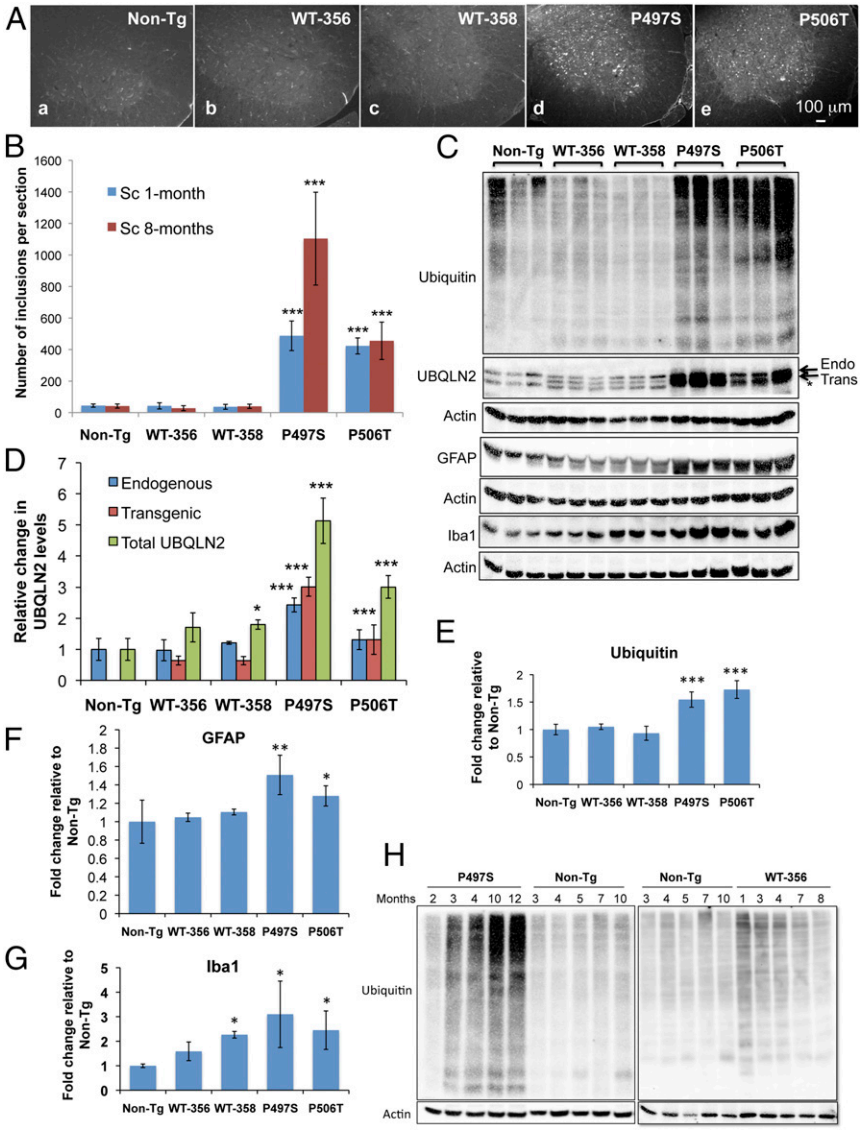

Fig. 3. Immunofluorescence and protein analyses of the SC of Tg animals. (*A*) UBQLN2 staining of the ventral horn of the SC in the different lines. (*B*) Quantification of UBQLN2 inclusions in SC sections in 1- and 8-mo-old Tg and non-Tg animals. (*C*) Immunoblots of SC lysates of 8-mo-old Tg and non-Tg animals (three independent mice) blotted for the antibodies shown. (*D*) Quantification of endogenous, Tg, and total UBQLN2 proteins in the blots shown in *C*. (*E*–*G*) Quantification of ubiquitin, GFAP, and Iba1 immunoreactivity in the blots shown in *C*. Data shown is the mean ± SEM. (*H*) Immunoblots of SC lysates of P497S, WT-356, and non-Tg mice (loaded for each comparison) of different ages for ubiquitin and actin loading.

P506T animals, compared with age-matched non-Tg animals (Fig. 3 *C* and *D* and *SI Appendix*, Fig. S3*C*). By contrast, the level of endogenous mUBQLN2 in both WT lines was not altered in animals of similar age. A simple explanation for this alteration is that mutant, but not WT UBQLN2, has slower turnover and slows turnover of endogenous mUBQLN2. Immunoblots of the same lysates revealed an elevation of ubiquitinated proteins in the mutant, but not WT lines, compared with non-Tg animals (Fig. 3 *C* and *E*). Further immunoblots of SC lysates made from mice of different ages revealed a progressive age-dependent increase of ubiquitinated proteins in P497S animals compared with the WT-356 line and the non-Tg mice control, suggesting that expression of P497S mtUBQLN2 protein induces a buildup of misfolded proteins over time (Fig. 3*H*).

We also examined the SCs of all of the animals to see whether there was a change in microglia and astrocyte activation in the lines. By both immunoblotting (Fig. 3 *C* and *F*) and changes in the intensity of immunofluoresecence staining (*SI Appendix*, Fig. S4 *A* and *B*) we found a significant increase in GFAP immunoreactivity, indicative of astrocytosis in both 8-mo-old P497S and P506T animals, compared with the age-matched non-Tg animals. This change did not manifest in the 1-mo-old animals (*SI Appendix*, Fig. S4*B*). Similar quantifications revealed a smaller, but a significant increase in GFAP reactivity in 8-mo-old animals in both the WT lines by measurements of the immunofluorescence staining intensity, but not by the blots, suggesting overexpression of UBQLN2 may be associated with some degree of astrocyte activation. Additionally, measurements of GFAP-staining intensity in 1-mo-old animals was very variable, but showed a trend of reduced staining in all of the Tg lines compared with non-Tg animals. Interestingly, there was a significant reduction of GFAP immunoreactivity in 1-mo-old animals in the WT-358 line. Repetition of the analysis for microglial activation using Iba1 reactivity revealed increased Iba1 immunoreactivity by immunoblot analysis in the two mutants (Fig. 3 *C* and *G*) and the WT-358 line at 8 mo of age compared with the non-Tg control. However, the immunofluorescence quantifications gave a different result, showing Iba1 immunoreactivity is increased in 8-mo-old P497S animals, and significantly decreased in P506T animals, compared with the non-Tg control (*SI Appendix*, Fig. S4 *A* and *C*). Further studies are needed to determine the cause of the variability in both GFAP and Iba1 reactivity seen in the different lines to see whether they are caused by differences in the stage of disease in the animals or from more localized changes in pathology of the animals.

Taken together the results suggest neuronal expression of mutant, but not WT UBQLN2 leads to an age-dependent increase

in UBQLN2 levels, inclusion formation, and ubiquitination of proteins in mice.

The Mouse Lines Expressing Mutant, but Not WT UBQLN2 Proteins Develop Clinical Signs of Motor Neuron Disease. To determine whether any of the Tg UBQLN2 lines develop any ALS-like disease, we tracked animal weight, grip strength, and latency to fall on an accelerating rotarod apparatus in mice from juvenile age to adulthood. Previous studies of SOD1 mouse models of ALS have shown that during disease progression, animals lose weight and show progressive decline in rotarod performance and grip strength (34–36). The body weight (Fig. 4*A*), rotarod (Fig. 4*B*), forelimb (Fig. 4*C*), and hindlimb (Fig. 4*D*) grip strength tests that were conducted at biweekly intervals for male and female mice starting from 6 to 32 wk of age for all four UBQLN2 Tg lines and non-Tg animals are shown (the data for males is shown in Fig. 4 and female data in *SI Appendix*, Fig. S5). The tests were terminated after 32 wk because of the difficulty in conducting the tests with the mtUBQLN2 lines. Statistical significant reductions in the outcomes of the tests for at least three consecutive periods are reported for male Tg mice compared with non-Tg mice, although females showed similar trends. Two-way ANOVA analysis of the data indicated both WT UBQLN2 lines did not differ from non-Tg mice in body weight, rotarod performance, and forelimb and hindlimb grip strength during the entire test period (from 6 to 32 wk of age). By contrast, P497S mtUBQLN2 mice had statistically significant reduction in body weight compared with non-Tg mice from 18 to 32 wk of age ($P \leq 0.05$ between 18–20 wk and $P \leq 0.001$ from 22 wk onward), whereas P506T males had significantly reduced body weight compared with the non-Tg mice after 26 wk of age ($P \leq 0.05$). Compared with non-Tg animals, P506T animals had noticeable reduction in rotarod performance and hindlimb grip strength at an early age (6 wk onward: $P \leq 0.001$ for all of the tests), which worsened over time. They also had reduced forelimb grip strength from 10 wk onward ($P \leq 0.05$). By contrast, P497S mice did not differ statistically in rotarod performance and forelimb grip strength from non-Tg mice until 12 and 24 wk of age, respectively, but thereafter their performance and strength got progressively worse ($P \leq 0.05$ for rotarod and $P \leq 0.01$ for the grip strength). However, like P506T mice, P497S mice had significant difference in hindlimb grip strength compared with non-Tg mice from 6 wk onward ($P \leq 0.001$). Taken together, the results indicated that the Tg mice expressing mutant, but not WT UBQLN2 protein develop progressive deficits in rotarod performance and weakness in both fore- and hindlimbs.

Tg Mice Expressing Mutant, but Not WT UBQLN2 Protein Develop Age-Dependent Motor-Neuron Disease. We next examined whether the deficits in rotarod performance and grip strength found in mutant P497S and P506T mice arise from loss of upper or lower motor neurons and/or from loss of innervation of the muscle. To examine these issues, we quantified the number of motor neurons in the ventral horn of the SC in the early-stage (~3-mo-old animals) and end-stage (~8 mo old) mtUBQLN2 mice, comparing them to those of age-matched WT and non-Tg animals using stereological principles. Motor neurons were identified in the ventral horn by their multipolar shape, large size (greater than 250 μm in area), and the presence of a prominent nucleolus following cresyl-violet staining (Fig. 5*A*) and their loss confirmed by choline acetyl transferase (ChAT) staining (*SI Appendix*, Fig. S6). The quantification revealed an age-dependent loss of motor neurons during end stage of disease in both P497S and P506T animals compared with age-matched non-Tg animals (Fig. 5*B*). By contrast, no motor neuron loss was evident in either of the two WT UBQLN2-expressing lines in animals of equivalent age as the end-stage mtUBQLN2 mice (Fig. 5*B*). Similarly, measurement of the weight of the gastrocnemius muscle revealed

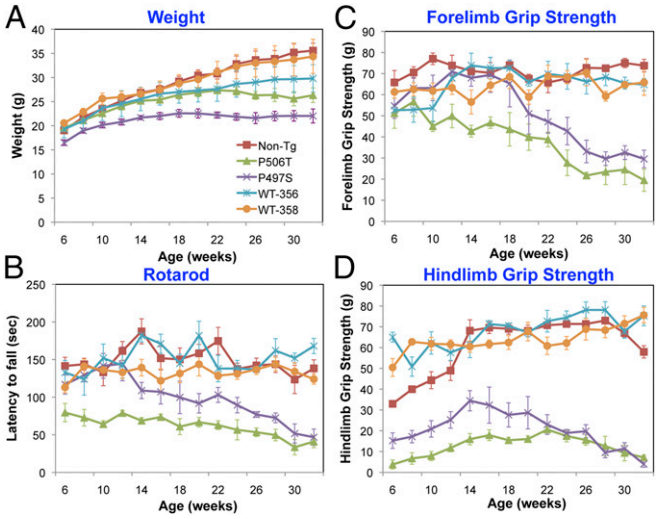

Fig. 4. Weight, rotarod, and grip strength analyses of the mice. (*A–D*) Biweekly analysis of weight, latency to fall on an accelerating rotarod apparatus, and grip strength for male mice (based on $N = 5–10$ animals) for the genotypes shown (color coded in *A*). The analysis was stopped at 32 wk due to poor performance of the mtUBQLN2 mice. Data shown are the mean ± SEM.

severe age-dependent muscle wasting in the two mutant UBQLN2-expressing lines compared with the non-Tg control (Fig. 5 *C* and *D*). The weight of the muscle in the WT-356 line was slightly lighter than non-Tg animals, but not as light as end-stage mtUBQLN2 animals. No such reduction was seen in the WT-358 line. Measurement of the diameter of individual fibers of the gastrocnemius muscle of the animals revealed that the mutant UBQLN2 mice at end stage had significantly smaller muscle fiber diameter compared with the two WT lines and non-Tg mice of equivalent age (Fig. 5*E*). Furthermore, many of the muscle fibers in the mutant lines were more triangular than rounded in shape and were frequently surrounded by numerous dark-stained nuclear bodies, suggestive of massive cellular infiltration of the degenerating fibers.

Measurement of the innervation of neuromuscular junctions of the gastrocnemius muscle, by analyzing the extent of colocalization of synatophysin and α-bungarotoxin labeling, revealed a significant age-dependent increase in denervation of the end plates in both the P497S and P506T lines (Fig. 6 *A–C* and *SI Appendix*, Fig. S7). By contrast, there was no loss in innervation of the muscle in either WT line or in the control non-Tg mice of similar age as the end-stage mtUBQLN2 mice (Fig. 6 *A* and *B*). Measurement of the number and cross-section area of myelinated axons in L4 roots of the mice further revealed a dramatic and significant age-dependent reduction of large-caliber axons (>70 μm^2 in size) in end-stage P497S and P506T UBQLN2 animals (Fig. 6 *D* and *E* and *SI Appendix*, Fig. S8 *B–D*). A comparison of the size distribution of axons in early-stage (~3 mo) and end-stage (~8 mo) animals revealed a large and significant reduction of large-caliber axons in both end-stage P497S and P506T lines, which was less evident in 3-mo-old animals (*SI Appendix*, Fig. S8 *A* and *D*). There was a shift in the size of the group of large-caliber axons in the WT-356 line at 8 mo of age, to slightly smaller axons, but the overall number of large-caliber axons appeared undiminished (Fig. 6*E* and *SI Appendix*, Fig. S8*D*). Similarly, there was no reduction in large-caliber axons in 8-mo-old animals in the WT-358 line. Interestingly, the peak of the group of small-caliber axons in both the WT-356 and WT-358 lines was double that found in non-Tg animals, which we speculate may represent some regeneration of axons in the animals.

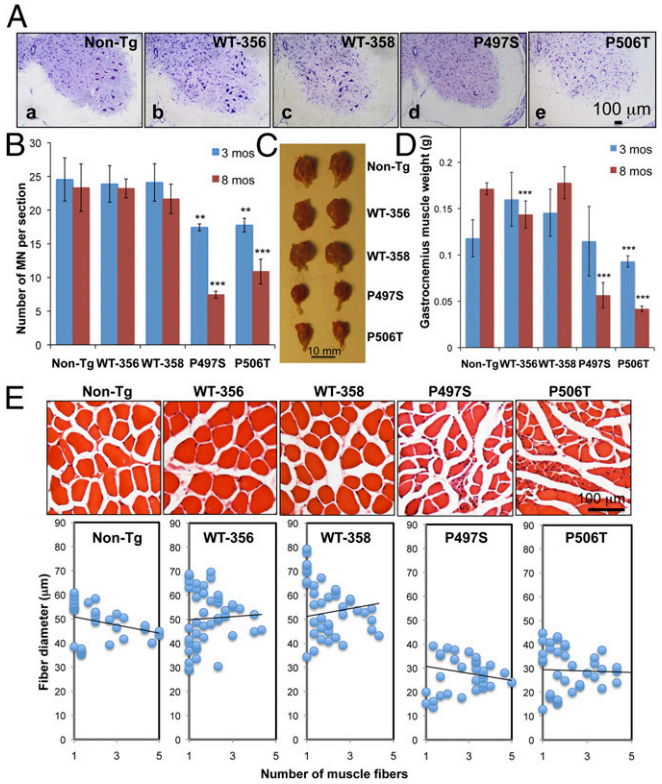

Fig. 5. Motor neuron loss and muscle wasting in the mtUBQLN2 mice. (*A*) Ventral horn sections of the SC stained with cresyl violet revealing loss of large-size motor neurons in mutant, but not WT UBQLN2 animals. (*B*) Quantification of motor neurons by stereology in the lumbar regions of the SCs in 3- and 8-mo-old animals. Data show means ± SEM. (*C*) Photos of the gastrocnemius muscle from both limbs of 8-mo-old mutant UBQLN2 mice and of equivalent age WT and non-Tg mice. (*D*) Graph showing the gastrocnemius muscle weight (averaged for one limb for three different animals) at 3 and 8 mo of age for the Tg and non-Tg animals. (*E*) Transverse sections of the gastrocnemius muscle stained with H&E. The fiber diameters of 100 fibers counted for each muscle are binned according to size for each genotype.

Because of the loss of lower motor neurons we examined ∼3- and 8-mo-old animals in all of the lines to determine whether there was similar loss of upper motor neurons. Coronal brain sections were stained with Ctip2 antibody to identify motor neurons and their numbers quantified using stereological principals. The data revealed little change in the number of corticospinal motor neurons in P497S and P506T animals compared with the non-Tg control (Fig. 7*A* and *SI Appendix*, Fig. S9). Surprisingly, however, there was a significant reduction of corticospinal motor neurons in the WT-356 animals at both 3 and 8 mo of age, but not in WT-358 animals. Although the exact reason for the loss of neurons in the WT-356 line remains unknown, the results suggest that overexpression of WT UBQLN2, but not the mutants, leads to some toxicity at least in corticospinal motor neurons.

Collectively the results indicate that overexpression of ALS–FTD mutant, but not WT UBQLN2 proteins leads to age-dependent motor neuron disease in mice.

P497S and P506T Mice Have Memory Deficits and Massive Neuronal Loss in the Hippocampus. Because UBQLN2 mutations cause ALS with FTD, we conducted behavioral tests to determine whether the mutant P497S and P506T Tg mice have any short-term and working memory impairments. We were cognizant that P497S and P506T Tg mice develop severe motor neuron disease during late stages of disease and for this reason only tested mice between 2 and 4 mo of age, avoiding any mouse with any noticeable deficit in movement. We also avoided physically difficult tests, such as swimming tasks. Because UBQLN2 inclusions accumulate in the hippocampus of the mutant lines, we focused on hippocampal-dependent cognitive tests involving novel object recognition (NOR) and the Y-maze test.

Measurement of the distance traveled in an open-field arena revealed there was no statistical difference between the two mutant and WT UBQLN2 lines compared with the non-Tg control used for the cognitive studies, indicating that any potential differences in the following behavioral tasks would not be due to differences in their locomotor and general exploratory activity (Fig. 7*C*).

We found no difference between any of the lines and non-Tg animals in spatial memory assessment as indicated by the lack of significant difference in the percentage of correct arm alternations in the Y-maze test (Fig. 7*D*). However, in the NOR test, non-Tg and WT-358 animals both discriminated the novel vs. familiar object ($P < 0.05$ vs. 0.5 threshold; Fig. 7*E*), whereas both P497S and P506T animals did not discriminate the novel vs. familiar object ($P > 0.05$ vs. 0.5 threshold; Fig. 7*E*). The discrimination ratio of the WT-356 animals was close to significance ($P = 0.056$), but we cannot rule out the possibility they have subtle memory impairments.

We next determined whether the Tg animals have any loss of neurons in the hippocampus. Accordingly, we quantified the number of $NeuN^+$ neurons in the dentate gyrus and CA1 regions in ∼3- (*SI Appendix*, Fig. S9) and 8-mo old animals (Fig. 7 *A* and *B*). The quantification revealed a significant reduction of neurons (∼40%) in both the CA1 and dentate gyrus in 8-mo-old Tg animals in both P497S and P506T lines compared with age-matched non-Tg control animals. By contrast, at 3 mo of age, there was less neuronal loss in the two brain regions in the P497S line, whereas there was significant, but reduced neuronal loss compared with 8-mo-old animals in the P506T line. Similar analysis of the WT lines revealed no neuronal loss in either brain region in the WT-358 line at both 3 and 8 mo of age, whereas WT-356 animals had no neuronal loss in the CA1 region, but had significant loss of neurons in the dentate gyrus at both 3 (*SI Appendix*, Fig. S9) and 8 mo of age (Fig. 7*A*).

We next conducted long-term potentiation (LTP) measurements of brain slices made from the same P506T and non-Tg animals where cognitive differences were found, but observed no difference in LTP between the two groups (*SI Appendix*, Fig. S10).

Abnormal Accumulation of TDP-43 Inclusions in the Cytoplasm of Motor Neurons in Mutant, but Not WT UBQLN2 Tg Mice. Because alteration of UBQLN2 expression was found to alter TDP-43 accumulation (32, 37) and because TDP-43 pathology manifests in spinal motor neurons in individuals harboring *UBQLN2* mutations (13, 15) we examined our UBQLN2 Tg mice to determine whether TDP-43 levels and/or its localization were altered in the SCs of 8-mo-old animals. Immunoblot analysis indicated TDP-43 protein levels were very variable in the three animals analyzed of the different genotypes, which we speculate may arise from differences in pathology or stage of disease in the mice (Fig. 8 *A* and *B*). Immunofluorescence detection of TDP-43 and UBQLN2 protein localization by confocal microscopy revealed diffuse TDP-43 staining that was much stronger in the nucleus compared with the cytoplasm in the large motor neurons of the SC in both WT-356 and WT-358 lines, which was similar to the staining pattern seen in non-Tg animals (Fig. 8*C* and *SI Appendix*, Fig. S11*A*). Double immunofluorescence staining of the same cells revealed UBQLN2 was distributed more uniformly across the entire cell, including the nucleus. By contrast, spinal motor neurons in end-stage (8 mo old) P497S and P506T Tg animals had reduced TDP-43 staining in the nucleus and many of the motor neurons

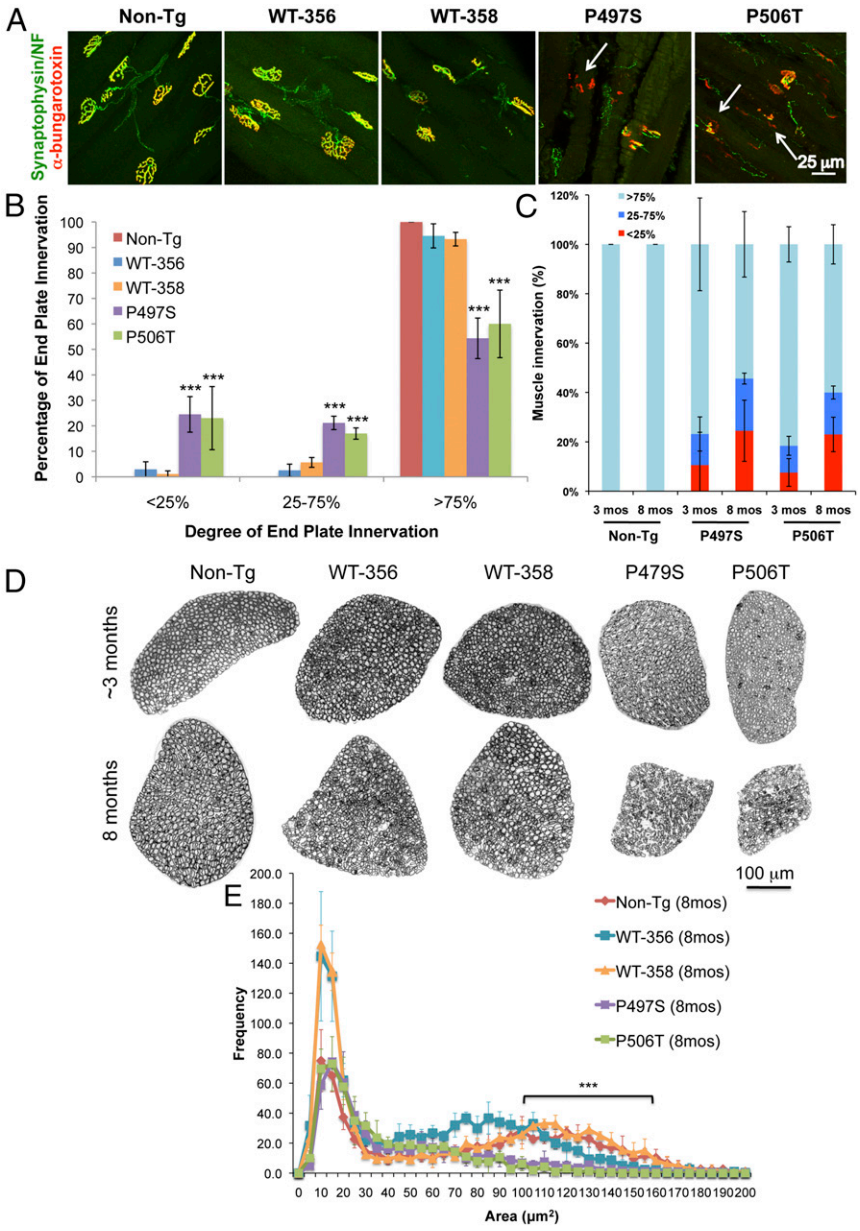

Fig. 6. Muscle denervation and loss of large-caliber axons in the L4 roots of mutant UBQLN2 Tg mice. (*A*) Colocalization of α-bungarotoxin (red fluorescence) and synaptophysin + neurofilament (green fluorescence) staining to identify innervated neuromuscular junctions. Arrows show end plates where there was poor-to-absent innervation. (*B*) Graph shows the percent of end plates with different degrees of innervation (>75%, 25–75%, and <25% overlap of the α-bungarotoxin and synaptophysin signals) in 8-mo-old animals. Data shown are the mean ± SD. (*C*) Quantification of the degree of colocalization of α-bungarotoxin and synaptophysin + neurofilaments as described in *C* compared in 3- and 8-mo-old mtUBQLN2 and non-Tg mice. (*D*) Transverse sections (1 μm) of the L4 roots in 3- and 8-mo-old Tg and non-Tg mice (same magnifications). (*E*) Histogram of the mean frequency ($n = 3$) of myelinated axons grouped according to their different areas into bins of 5 μm for the different genotypes. Two-way ANOVA indicated a specific reduction of large-caliber axons (between 100 and 160 μm^2 in area) in the mtUBQLN2 mice.

contained granular inclusions with strong staining for TDP-43 that appeared to be clustered in the cytoplasm (Fig. 8*C* and *SI Appendix*, Fig. S11*B*). The inclusions were also positive for UBQLN2 staining, but the UBQLN2 signal was weaker. Further double immunofluorescence staining revealed that the TDP-43 inclusions were positive for ubiquitin (Fig. 8*D*). We next examined SCs of 3-mo-old P497S and P506T animals to determine whether the TDP-43 pathology occurs at an earlier age. However, we did not detect any reduction in TDP-43 staining in the nucleus or the formation of cytoplasmic TDP-43 inclusions in motor neurons at this early time point (*SI Appendix*, Fig. S12*A*).

We next examined P497S and P506T end-stage animals for TDP-43 pathology in the hippocampus, a region of the brain where numerous UBQLN2 aggregates form, but found no evidence for any signs of the pathology in the cells of the dentate gyrus (*SI Appendix*, Fig. S12 *B* and *C*). Furthermore, double immunofluorescence staining of the sections revealed the UBQLN2 aggregates in the dentate gyrus were negative for TDP-43 staining.

In summary, these results indicate that P497S and P506T mutant UBQLN2 mice with end stage of disease display a reduction of TDP-43 staining in the nucleus with concomitant formation of cytoplasmic ubiquitin$^+$ inclusions in spinal motor neurons. The alteration in TDP-43 staining we observed in the Tg models are a classical pathological signature found in the vast majority of human ALS cases (5–7).

Discussion

Here we describe two Tg mouse lines that carry the P497S or P506T *UBQLN2* mutation, both of which develop motor neuron disease and cognitive deficits together with pathological accumulation of UBQLN2 inclusions in the SC and dentate gyrus of the brain, combined with TDP-43 pathology in spinal motor neurons. Both lines had shorter lifespan compared with non-Tg animals. The mean lifespan of mice for the P497S line was 246 d and 305 d for the P506T line. End-stage animals in both lines had dramatic loss of lower motor neurons, denervation of muscle end plates, muscle wasting, reduction of muscle fiber diameter,

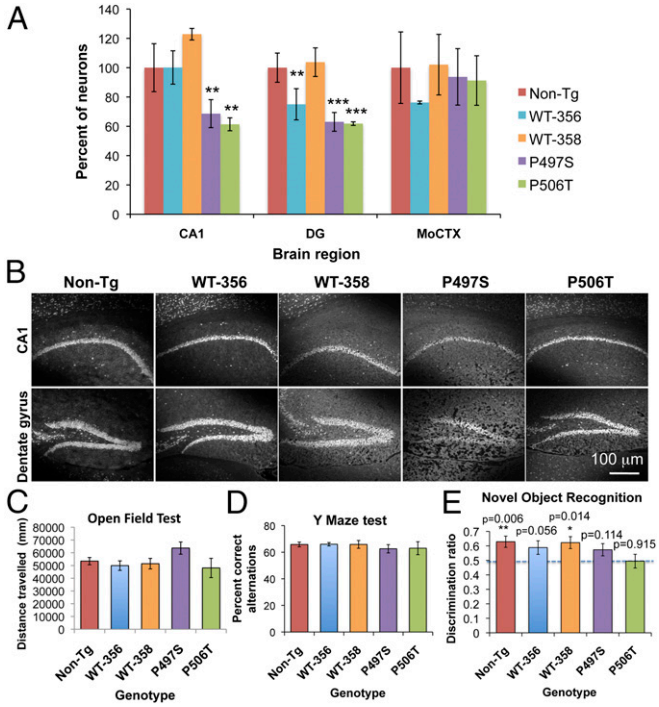

Fig. 7. Cognitive deficits and loss of neurons in the hippocampus in mtUBQLN2 mice. (*A*) Stereological neuronal counts of NeuN$^+$ cells in the CA1 and dentate gyrus and of Ctip2$^+$ cells in the motor cortex in the different lines. Data shown are the mean ± SEM. (*B*) Representative images of the CA1 and dentate gyrus (staining with NeuN) in coronal sections taken from the mice with the genotypes shown. (*C–E*) Cognitive tests. All of the tests shown were done with the same group of animals: 14 non-Tg, 12 WT-356, 12 WT-358, 11 P497S, and 7 P506T between 2 and 3 mo of age. The tests with the WT animals were done at a different time from the other groups. (*C*) Open-field analysis showing no statistical difference between Tg and non-Tg animals. (*D*) There was no difference in the percentage of alternations made in the Y-maze test in any of the lines tested. (*E*) NOR test showing non-Tg and WT-358 mice have higher ratio of discrimination of a novel to a familiar object compared with P497S, P506T, or WT-356 animals.

astrocytosis, and loss of neurons in the hippocampus (38, 39). The high degree to which the models recapitulate the clinical and pathological phenotypes of humans with *UBQLN2* mutations make them extremely useful for understanding the mechanisms underlying ALS–FTD and for testing therapies to prevent disease.

In contrast with our results, other rodent models expressing the ALS–FTD-linked P497H or P506T UBQLN2 mutation developed only cognitive, but not motor neuron disease (19, 27, 29). The reason for the difference is not clear. One likely possibility is that the level of mtUBQLN2 expression required to induce motor neuron disease needs to be higher than was achieved in the other rodent models. In one of these models, the same P506T *UBQLN2* mutation carried by one of our models was knocked in at an equivalent position in the mouse UBQLN2 gene, yet those mice did not develop motor neuron disease (19). This would suggest that the mouse UBQLN2 gene is either expressed at lower levels than in humans and/or that despite their similar expression, the very short lifespan of mice compared with humans is insufficient for motor neuron disease to manifest. A similar reasoning may explain why the mouse model expressing the P497H mutation driven by the endogenous mouse UBQLN2 gene promoter failed to develop motor neuron disease (29). The third case may have arisen from use of a CaMKα2 promoter to drive mutant P497H UBQLN2 expression, which might have been too restrictive in tissue expression (27). The mtUBQLN2 proteins expressed in our mice were with the Thy1.2 promoter, which is known to drive Tg expression only in neurons throughout the central and peripheral nervous system (33). Regardless of the reason, our results indicate that neuron-specific expression of mutant UBQLN2 proteins is sufficient to induce ALS and FTD-like symptoms in mice. It will be important for future studies to examine whether expression of the UBQLN2 mutants in cells other than, or in addition to neurons such as astrocytes, microglia or oligodendrocytes will cause or exacerbate ALS–FTD symptoms.

In another study where mouse lines were not generated, WT and mutant UBQLN2 proteins were ectopically expressed in mice following intracerebroventricular injection of recombinant AAV (31). Several of the injected mice developed UBQLN inclusions in the brain and those injected with constructs encoding P497S and P506T mtUBQLN2 proteins had compromised rotarod performance at 3 mo of age compared with mice injected with constructs encoding WT or P497H UBQLN2 proteins. However, the AAV-injected animals were not studied for motor neuron disease so the underlying reason for the motor deficit in the mice remains unknown. Nevertheless, the findings are in agreement with our results showing that expression of the P497S and P506T mtUBQLN2 proteins are toxic.

An obvious question regarding the disease symptoms that develop in our P497S and P506T Tg lines are whether they are a manifestation of overexpression of hUBQLN2 protein per se or the intrinsic property of the mutations. Based on lack of development of motor neuron disease in the two WT hUBQLN2-expressing lines, one of which (line WT-356) had similar levels of hUBQLN2 overexpressed as the mutant lines that developed disease, it is apparent that the motor neuron disease phenotype derives from the expression of the UBQLN2 mutations rather than from simple overexpression of hUBQLN2 protein. However, we should caution that the overexpression of WT hUBQLN2 in neurons was not without effect. We observed some loss of upper motor neurons and loss of neurons in the dentate gyrus in the WT-356 line, suggesting that overexpression of WT hUBQLN2 is indeed associated with some toxicity, albeit reduced compared with the mutant hUBQLN2 proteins. Also, the axonal caliber profile in both the WT lines was altered by an increase in small-caliber axons and a general shift of the large-caliber axons to slightly smaller axons in the WT-356 line, compared with non-Tg animals. These changes suggest that overexpression of WT UBQLN2 is associated with some toxicity. Interestingly, overexpression of WT UBQLN2 was recently shown to induce neurodegenerative phenotypes and pathology in the brain similar to the expression of mutant P497H UBQLN2 protein (40). The capacity of WT hUBQLN2 to induce toxicity when highly overexpressed is consistent with an increase in cell death seen upon overexpression of the protein in cell cultures, although like our animal studies, there too, toxicity of the WT protein was less potent than ALS–FTD mutant UBQLN2 proteins (30, 41). The toxicity caused by overexpression of WT UBQLN2 is not entirely surprising because overexpression of WT *SOD1*, *TDP43*, and *FUS*, all of which are encoded by genes in which mutations cause ALS, generate disease phenotypes (42–44). Obviously, the mechanism by which overexpression of these different WT proteins cause disease may be unrelated.

The behavioral deficits that developed in the UBQLN2 Tg lines correlated well with the pathologic changes we observed in the animals, particularly in the mutant P497S and P506T lines. The progressive decrease in rotarod performance and grip strength in the mutant lines was associated with progressive loss of motor neurons in the SC and in denervation of the endplates in the muscle of the animals. Likewise, the deficiency in cognition revealed by changes in NOR was associated with the striking loss of neurons in the dentate gyrus and CA1 regions of the hippocampus in the end-stage mtUBQLN2 animals. The possible deficit in cognition in the WT-356 line could also be related

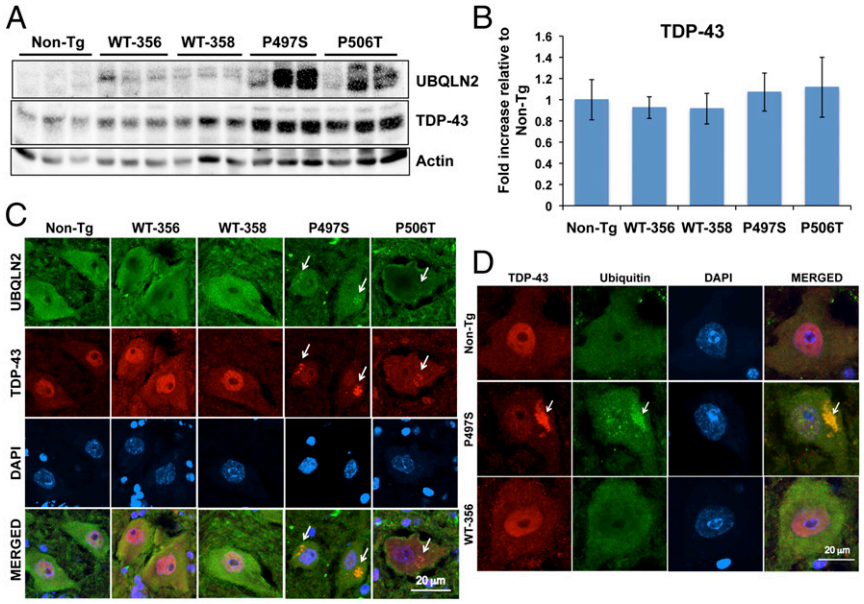

Fig. 8. TDP-43 pathology in mtUBQLN2 mice. (*A*) Immunoblots of SC lysates from 8-mo-old Tg and non-Tg mice blotted for the proteins shown. (*B*) Quantification of TDP-43 levels in the blots shown in *A*. Data shown are the mean ± SEM. (*C*) Confocal microscopy of TDP-43, UBQLN2, and DAPI staining, and a merged image of all three stainings in motor neurons in the ventral horn of the SC in the Tg and non-Tg mice. The arrows indicate TDP-43^{+} inclusions in the cytoplasm that were also positive for UBQLN2. (*D*) Similar to *C*, but stained for TDP-43, ubiquitin, and DAPI. Arrows indicate inclusions that were positive for TDP-43 and ubiquitin.

to loss of neurons of the dentate gyrus in the animals, but this appeared to be independent of any noticeable appearance of UBQLN2 inclusions. We did not find any changes in LTP measurements in hippocampal recordings between non-Tg and P506T animals, unlike the reported change in Tg mice expressing the P497H mutation (29). The reason for the difference is not clear, but may be related to a technical or the genotype difference in the animals studied. In our study, we found no difference in the LTP in P506T animals that had performed poorly in the cognitive tests. It is possible that an LTP difference may manifest in more-aged animals.

A particularly striking feature of the pathology seen in the brains of the affected mtUBQLN2 mice was the plethora of UBQLN2 inclusions that accumulated in an age-dependent manner in a distinctive but reproducible pattern in both lines. The reproducibility of the pattern in these and other UBQLN2 rodent models constructed using different promoters suggests either the organization or system of neurons where they are found are more capable and/or resistant to the expression and accumulation of the UBQLN2 inclusions.

Several sites in the brain where ubiquilin inclusions were found were associated with massive neuronal loss in end-stage P497S and P506 animals, suggesting a possible connection between accumulation of UBQLN2 inclusions and neuronal demise. Previous studies have shown that mtUBQLN2 proteins interfere with proteasomal degradation by retaining their ability to bind polyubiquitinated proteins, but inability to deliver the bound proteins to the proteasome for degradation from a failure to dock with the proteasome (30, 32). Studies also suggest the mtUBQLN2 proteins interfere with autophagy (32). Thus, the age-dependent buildup of UBQLN2 inclusions in the mutant lines is consistent with dominant interference of misfolded protein clearance through the proteasome and/or autophagy pathways. Consistent with such defective clearance of misfolded proteins, the inclusions stained positive for ubiquitin and thioflavin S, a dye that binds aggregate-prone proteins that assemble into higher order amyloid conformations. The interference in protein degradation by mtUBQLN2 proteins highlights the importance that disturbances in protein homeostasis (proteostasis) may play in pathogenesis of ALS–FTD.

A remarkable pathological feature found in the mutant UBQLN2 lines was the presence of TDP-43 pathology (i.e., a reduction of TDP-43 staining in the nucleus and accumulation in cytoplasmic inclusions that were ubiquitin^{+}) in spinal motor neurons in animals at end stage of disease (~8 mo of age). This pathology was not found in equivalent-age animals in either WT line or in the 3-mo-old P497S or P506T mutant animals. The development of TDP-43 pathology at late stages of disease suggests the pathology is intimately connected, either directly or indirectly, to disease pathogenesis of motor neurons. There is considerable investigation in the ALS field to determine the exact link between TDP-43 pathology and motor neuron demise. It will be interesting in the future to determine the exact time course of the TDP-43 pathology in the mutant UBQLN2 lines and to determine its involvement in motor neuron disease.

There is variance as to whether TDP-43 is present in the UBQLN2 inclusions that form in the brain in rodent models of UBQLN2, with two reports demonstrating it is not present (13, 27) and one that showed it was present (31). Using a C-terminal TDP-43–specific antibody we did not detect any evidence for TDP-43 in the UBQLN2 inclusions that decorate the dentate gyrus of the brains in our mutant UBQLN2 mice. However, we did detect colocalization of TDP-43 and UBQLN2 in the cytoplasmic inclusions that were formed in spinal motor neurons during end stage of disease in both mutant lines. Further investigation is needed to determine why UBQLN2 is present in some, but not all inclusions.

A central question in neurodegenerative diseases, and for that matter ALS, is why specific symptoms manifest in the different disorders despite ubiquitous or similar expression patterns of many of the mutant genes. Although, our results do not provide a definitive answer to this question, they provide clues about the vulnerability of motor neurons in ALS. Our results demonstrate motor neurons are highly susceptible to death caused by overexpression of the mutant UBQLN2 proteins. We speculate that this susceptibility is because they are vulnerable to disturbances

in proteostasis, based on the defective properties of mutant UBQLN2 proteins and by extrapolation from other studies. First, our results, like those of others studies, clearly show the UBQLN2 mutants disrupt proteostasis, leading to accumulation of misfolded proteins (13, 28–31). Second, accumulating evidence suggests disturbance in proteostasis, particularly induction of the UPR, as central in disease pathogenesis caused by ALS mutations in *SOD1* and *C9ORF72* (45–49). Furthermore, disruption of proteasome function in motor neurons in mice leads to ALS-like pathology (50). Collectively, the results suggest motor neurons may be especially vulnerable to insult caused by disturbances in proteostasis. It will be important in the future to decipher the mechanistic relationship between dysfunction in proteostasis caused by UBQLN2 mutations and TDP-43 pathology that develops in the mice and their link to ALS pathogenesis.

In summary, we have shown that the two P497S and P506T mutant UBQLN2 Tg mouse lines we have developed recapitulate the central features of ALS–FTD found in humans. These mice, together with the Tg lines expressing WT UBQLN2 proteins that do not develop motor neuron disease provide extremely useful models for deciphering the mechanisms by which UBQLN2 mutations cause ALS–FTD, as well as for testing therapeutics to halt the disease.

Materials and Methods

cDNA encoding either WT or ALS–FTD mutant untagged human UBQLN2 proteins were cloned into the Thy1.2 expression cassette and Tg mice were generated following pronuclear injection of fertilized mouse embryos. The detailed methods for the characterization of mouse lines carrying either the WT or ALS–FTD mutant P497S or P506T transgenes are provided in *SI Appendix*. All the animal studies were done in accordance with the NIH Guide for the Care and Use of Laboratory Animals (51) and approved by the Institutional Animal Care and Use Committee of the University of Maryland, Baltimore.

ACKNOWLEDGMENTS. We thank Dr. Pico Caroni for providing the Thy1.2 expression cassette and Drs. Liron Boyman and Andrew Ziman for help with the confocal microscopy. This work was supported in part by a grant from the Robert Packard Center for ALS Research at Johns Hopkins (to M.J.M.).

1. Rowland LP, Shneider NA (2001) Amyotrophic lateral sclerosis. *N Engl J Med* 344(22): 1688–1700.
2. Kiernan MC, et al. (2011) Amyotrophic lateral sclerosis. *Lancet* 377(9769):942–955.
3. Robberecht W, Philips T (2013) The changing scene of amyotrophic lateral sclerosis. *Nat Rev Neurosci* 14(4):248–264.
4. Ling SC, Polymenidou M, Cleveland DW (2013) Converging mechanisms in ALS and FTD: Disrupted RNA and protein homeostasis. *Neuron* 79(3):416–438.
5. Neumann M, et al. (2006) Ubiquitinated TDP-43 in frontotemporal lobar degeneration and amyotrophic lateral sclerosis. *Science* 314(5796):130–133.
6. Arai T, et al. (2006) TDP-43 is a component of ubiquitin-positive tau-negative inclusions in frontotemporal lobar degeneration and amyotrophic lateral sclerosis. *Biochem Biophys Res Commun* 351(3):602–611.
7. Mackenzie IR, et al. (2007) Pathological TDP-43 distinguishes sporadic amyotrophic lateral sclerosis from amyotrophic lateral sclerosis with SOD1 mutations. *Ann Neurol* 61(5):427–434.
8. Scotter EL, Chen HJ, Shaw CE (2015) TDP-43 proteinopathy and ALS: Insights into disease mechanisms and therapeutic targets. *Neurotherapeutics* 12(2):352–363.
9. Seelaar H, et al. (2010) Frequency of ubiquitin and FUS-positive, TDP-43-negative frontotemporal lobar degeneration. *J Neurol* 257(5):747–753.
10. Urwin H, et al.; FReJA Consortium (2010) FUS pathology defines the majority of tau- and TDP-43-negative frontotemporal lobar degeneration. *Acta Neuropathol* 120(1):33–41.
11. Van Langenhove T, van der Zee J, Van Broeckhoven C (2012) The molecular basis of the frontotemporal lobar degeneration-amyotrophic lateral sclerosis spectrum. *Ann Med* 44(8):817–828.
12. Mackenzie IR, Neumann M (2016) Molecular neuropathology of frontotemporal dementia: Insights into disease mechanisms from postmortem studies. *J Neurochem* 138 (Suppl 1):54–70.
13. Deng HX, et al. (2011) Mutations in UBQLN2 cause dominant X-linked juvenile and adult-onset ALS and ALS/dementia. *Nature* 477(7363):211–215.
14. Gellera C, et al.; SLAGEN Consortium (2013) Ubiquilin 2 mutations in Italian patients with amyotrophic lateral sclerosis and frontotemporal dementia. *J Neurol Neurosurg Psychiatry* 84(2):183–187.
15. Williams KL, et al. (2012) UBQLN2/ubiquilin 2 mutation and pathology in familial amyotrophic lateral sclerosis. *Neurobiol Aging* 33(10):2527.e3-10.
16. Fahed AC, et al. (2014) UBQLN2 mutation causing heterogeneous X-linked dominant neurodegeneration. *Ann Neurol* 75(5):793–798.
17. Kaye FJ, et al. (2000) A family of ubiquitin-like proteins binds the ATPase domain of Hsp70-like Stch. *FEBS Lett* 467(2–3):348–355.
18. Itakura E, et al. (2016) Ubiquilins chaperone and triage mitochondrial membrane proteins for degradation. *Mol Cell* 63(1):21–33.
19. Hjerpe R, et al. (2016) UBQLN2 mediates autophagy-independent protein aggregate clearance by the proteasome. *Cell* 166(4):935–949.
20. Kim TY, Kim E, Yoon SK, Yoon JB (2008) Herp enhances ER-associated protein degradation by recruiting ubiquilins. *Biochem Biophys Res Commun* 369(2):741–746.
21. Lim PJ, et al. (2009) Ubiquilin and p97/VCP bind erasin, forming a complex involved in ERAD. *J Cell Biol* 187(2):201–217.
22. Gilpin KM, Chang L, Monteiro MJ (2015) ALS-linked mutations in ubiquilin-2 or hnRNPA1 reduce interaction between ubiquilin-2 and hnRNPA1. *Hum Mol Genet* 24(9):2565–2577.
23. Rothenberg C, Monteiro MJ (2010) Ubiquilin at a crossroads in protein degradation pathways. *Autophagy* 6(7):979–980.
24. Lee DY, Brown EJ (2012) Ubiquilins in the crosstalk among proteolytic pathways. *Biol Chem* 393(6):441–447.
25. N'Diaye EN, et al. (2009) PLIC proteins or ubiquilins regulate autophagy-dependent cell survival during nutrient starvation. *EMBO Rep* 10(2):173–179.
26. Rothenberg C, et al. (2010) Ubiquilin functions in autophagy and is degraded by chaperone-mediated autophagy. *Hum Mol Genet* 19(16):3219–3232.
27. Wu Q, et al. (2015) Pathogenic Ubqln2 gains toxic properties to induce neuron death. *Acta Neuropathol* 129(3):417–428.
28. Xia Y, et al. (2014) Pathogenic mutation of UBQLN2 impairs its interaction with UBXD8 and disrupts endoplasmic reticulum-associated protein degradation. *J Neurochem* 129(1):99–106.
29. Gorrie GH, et al. (2014) Dendritic spinopathy in transgenic mice expressing ALS/dementia-linked mutant UBQLN2. *Proc Natl Acad Sci USA* 111(40):14524–14529.
30. Chang L, Monteiro MJ (2015) Defective proteasome delivery of polyubiquitinated proteins by Ubiquilin-2 proteins containing ALS mutations. *PLoS One* 10(6):e0130162.
31. Ceballos-Diaz C, et al. (2015) Viral expression of ALS-linked ubiquilin-2 mutants causes inclusion pathology and behavioral deficits in mice. *Mol Neurodegener* 10:25.
32. Osaka M, Ito D, Suzuki N (2016) Disturbance of proteasomal and autophagic protein degradation pathways by amyotrophic lateral sclerosis-linked mutations in ubiquilin 2. *Biochem Biophys Res Commun* 472(2):324–331.
33. Caroni P (1997) Overexpression of growth-associated proteins in the neurons of adult transgenic mice. *J Neurosci Methods* 71(1):3–9.
34. Gurney ME, et al. (1994) Motor neuron degeneration in mice that express a human Cu,Zn superoxide dismutase mutation. *Science* 264(5166):1772–1775.
35. Bruijn LI, et al. (1997) ALS-linked SOD1 mutant G85R mediates damage to astrocytes and promotes rapidly progressive disease with SOD1-containing inclusions. *Neuron* 18(2):327–338.
36. Vinsant S, et al. (2013) Characterization of early pathogenesis in the SOD1(G93A) mouse model of ALS: Part I, background and methods. *Brain Behav* 3(4):335–350.
37. Cassel JA, Reitz AB (2013) Ubiquilin-2 (UBQLN2) binds with high affinity to the C-terminal region of TDP-43 and modulates TDP-43 levels in H4 cells: Characterization of inhibition by nucleic acids and 4-aminoquinolines. *Biochim Biophys Acta* 1834(6):964–971.
38. Zinszner H, et al. (1998) CHOP is implicated in programmed cell death in response to impaired function of the endoplasmic reticulum. *Genes Dev* 12(7):982–995.
39. Marciniak SJ, et al. (2004) CHOP induces death by promoting protein synthesis and oxidation in the stressed endoplasmic reticulum. *Genes Dev* 18(24):3066–3077.
40. Huang B, Wu Q, Zhou H, Huang C, Xia XG (2016) Increased Ubqln2 expression causes neuron death in transgenic rats. *J Neurochem* 139(2):285–293.
41. Graffmo KS, et al. (2013) Expression of wild-type human superoxide dismutase-1 in mice causes amyotrophic lateral sclerosis. *Hum Mol Genet* 22(1):51–60.
42. Xu YF, et al. (2010) Wild-type human TDP-43 expression causes TDP-43 phosphorylation, mitochondrial aggregation, motor deficits, and early mortality in transgenic mice. *J Neurosci* 30(32):10851–10859.
43. Wils H, et al. (2010) TDP-43 transgenic mice develop spastic paralysis and neuronal inclusions characteristic of ALS and frontotemporal lobar degeneration. *Proc Natl Acad Sci USA* 107(8):3858–3863.
44. Mitchell JC, et al. (2013) Overexpression of human wild-type FUS causes progressive motor neuron degeneration in an age- and dose-dependent fashion. *Acta Neuropathol* 125(2):273–288.
45. Nishitoh H, et al. (2008) ALS-linked mutant SOD1 induces ER stress- and ASK1-dependent motor neuron death by targeting Derlin-1. *Genes Dev* 22(11):1451–1464.
46. Saxena S, Cabuy E, Caroni P (2009) A role for motoneuron subtype-selective ER stress in disease manifestations of FALS mice. *Nat Neurosci* 12(5):627–636.
47. Wang L, Popko B, Tixier E, Roos RP (2014) Guanabenz, which enhances the unfolded protein response, ameliorates mutant SOD1-induced amyotrophic lateral sclerosis. *Neurobiol Dis* 71:317–324.
48. Das I, et al. (2015) Preventing proteostasis diseases by selective inhibition of a phosphatase regulatory subunit. *Science* 348(6231):239–242.
49. Prudencio M, et al. (2015) Distinct brain transcriptome profiles in C9orf72-associated and sporadic ALS. *Nat Neurosci* 18(8):1175–1182.
50. Tashiro Y, et al. (2012) Motor neuron-specific disruption of proteasomes, but not autophagy, replicates amyotrophic lateral sclerosis. *J Biol Chem* 287(51):42984–42994.
51. Committee on Care and Use of Laboratory Animals (1996) Guide for the Care and Use of Laboratory Animals (Natl Inst Health, Bethesda), DHHS Publ No (NIH) 85–23.